Isı Bilimi ve Tekniği Dergisi, 30, 2, 21-35, 2010
J. of Thermal Science and Technology

ISSN 1300-3615

EXPERIMENTAL AND COMPUTATIONAL INVESTIGATION OF VELOCITY FIELD FOR INTERMEDIATE REGION OF LAMINAR PULSATILE PIPE FLOW

Fuat YILMAZ and Mehmet Yasar GUNDOGDU*
Department of Mechanical Engineering, University of Gaziantep, 27310, Gaziantep, Turkey
fuatyilmaz@gantep.edu.tr, gundogdu@gantep.edu.tr (*Corresponding author)

(Geliş Tarihi: 25. 05. 2009, Kabul Tarihi: 01. 12. 2009)

Abstract: In this study, velocity field in intermediate region of laminar-pulsatile pipe flow is investigated by using experimental and computational techniques. Initially, variations of cross sectional velocity profile and static pressure difference at a test section through 30 different instants of a pulsation cycle are measured respectively by means of a hot-wire anemometer and a pressure transducer for 29 different runs covering the ranges; $2.26x10^3\pm17\%\leq Re_{ta}\leq 4.36x10^3\pm10\%$, $5.1\pm4\%\leq\sqrt{\omega}\leq 28.0\pm0.05\%$, $0.03\leq A_1\leq 0.71$. Selected four different ones of the experimental runs are then analyzed computationally by using the finite-volume based Fluent software-package. The results of both experimental and computational parts of this study indicate that the general tendencies of dimensionless velocity profiles are very similar to the Blasius's distribution but differ appreciably from the Prandtl's distribution for the all runs in intermediate region of laminar-pulsatile pipe flow. Both the experimental and the computational velocity profiles become blunter than the Blasius's distribution in some phases of the pulsation cycle but become sharper than it in the remaining phases for the all runs.
Keywords: Pulsatile pipe flow, Laminar, Intermediate region, Velocity, Pressure, CFD.

LAMİNAR DARBELİ BORU AKIŞININ ARA BÖLGESİ İÇİN HIZ ALANININ DENEYSEL VE HESAPLAMALI OLARAK İNCELENMESİ

Özet: Bu çalışmada, laminar-darbeli boru akışının ara bölgesindeki hız alanı deneysel ve hesaplamalı teknikler kullanılarak incelenmiştir. Öncelikle, bir test bölgesindeki kesitsel hız dağılımının ve statik basınç farkının bir darbe çeviriminin 30 farklı anındaki değişimleri, sırasıyla bir kızgın-tel anemometresi ve bir basınç transdüseri kullanarak 29 farklı çalışma şartını kapsayacak şekilde ($2.26x10^3\pm17\%\leq Re_{ta}\leq 4.36x10^3\pm10\%$, $5.1\pm4\%\leq\sqrt{\omega}\leq 28.0\pm0.05\%$, $0.03\leq A_1\leq 0.71$), ölçülmüştür. Daha sonra, deneysel şartların birbirinden farklı seçilmiş dört tanesi, sonlu-hacim tabanlı Fluent yazılım programı vasıtasıyla, hesaplamalı olarak analiz edilmiştir. Hem hesaplamalı hem de deneysel çalışmaların neticeleri göstermektedir ki; laminar-darbeli boru akışının ara bölgesindeki bütün şartlar için boyutsuz hız profillerinin genel eğilimleri Blasius'un dağılımına çok benzemekte fakat Prandtl'ın dağılımından önemli ölçüde farklılık göstermektedir. Bütün deney şartları için hem deneysel hem de hesaplamalı hız profilleri bir darbe çevriminin bazı fazlarında Blasus'un dağılımından daha küt olmakta fakat kalan fazlarda ondan daha keskin olmaktadır.
Anahtar Kelimeler: Darbeli boru akışı, Laminar, Ara bölge, Hız, Basınç, HAD.

NOMENCLATURE

A_1	: velocity amplitude ratio [$=U_{m,os,1}/U_{m,ta}$]
D	: pipe diameter [m]
L	: axial distance [m]
ΔP	: pressure difference [Pa]
dP/dx	: static pressure gradient [Pa/m]
$\Delta P/L$	: approximate static pressure gradient [Pa/m]
r	: radial distance [m]
R	: pipe radius [m]
R^2	: coefficient of determination
Re_{ta}	: Re number based on time-averaged value of cross-sectional mean velocity [$=U_{m,ta}D/\upsilon$]
t	: time [sec]
T	: period of oscillation [1/s]
u	: axial velocity [m/s]
U_{cl}	: centerline velocity [m/s]
U_m	: cross-sectional mean velocity [m/s]
$U_{m,ta}$	: time-averaged value of cross-sectional mean velocity [m/s]
$\lvert U_{m,os,1}\rvert$	: amplitude of oscillatory cross-sectional mean velocity for the fundamental wave in the finite Fourier expansion [m/s]
v	: radial velocity [m/s]
x	: axial coordinate [m]
υ	: kinematic viscosity [m^2/s]
ρ_0	: density at t=0 [kg/m^3]
ω	: angular frequency of oscillation [rad/s] ; [$=2\pi/T$]

$\sqrt{\omega'}$: dimensionless frequency parameter (i.e., Strouhal number, Womersley parameter, Ohmi parameter) ;[$=R(\omega/\upsilon)^{1/2}$]

$\sqrt{\omega'_q}$: limiting dimensionless frequency between quasi-steady and intermediate regions

$\sqrt{\omega'_t}$: limiting dimensionless frequency between intermediate and inertia dominant regions

Subscripts and others:

m : cross sectional mean value
os : oscillatory component due to pulsation
ta : long time-averaged values
1 : fundamental wave in the finite Fourier expansion
_ : ensemble-averaged value
$\angle$: phase angle [^{0}]

INTRODUCTION

Pulsatile flow is composed of a positive mean and a periodically varying time-dependent component (generally sinusoidal as in nature) around the mean, whereas in oscillatory flow, time-dependent component varies around a zero mean. Investigation of these flows has of great importance especially in the biomedical science and industry. Physical characteristics of blood flow orient the researchers towards blood rheology for well analysis of the arterial blood flow (Yilmaz and Gundogdu, 2008; Yilmaz and Gundogdu, 2009). Understanding the mechanisms of pulse generation through the pipe lines including the devices operating on reciprocating motion such as positive displacement pumps and compressors, and the fittings such as vanes, valves, junctions, etc. has also very critical. Furthermore, inertia dominant character of pulsatile pipe flow has been used as a good choice for the prevention of widely observed obstruction and choking problems through two- or multi-phase flow lines such as waste-water lines, drainage (slurry) lines, and pneumatic conveying lines.

Pulsatile and oscillatory flows in laminar regime which are two representative types of unsteady flow have been studied theoretically and experimentally since the first quarter of 20th century and these investigations were reviewed in great detail (Gundogdu and Carpinlioglu, 1999; Carpinlioglu and Gundogdu, 2001a). Analytical and numerical solutions of the continuity, momentum, and energy equations for fluids of any kind are relatively rare due to the mathematical complexities. Analytical solutions are particularly difficult because of the increased dimensionality (Sexl, 1930; Szymanski, 1932; Womersley, 1955, 1957; Uchida, 1956; Linke and Hufschmidt, 1958; Hershey and Song, 1967; Ohmi et al., 1981a, 1981b; Donovan et al., 1991, 1994). Approximate solutions are based on modified and simplified equivalent viscosity representations for Newtonian fluids (Atabek and Chang, 1961; Brown, 1962; D'Souza and Olderburger, 1964; Zielke, 1968; Jayasinghe et al., 1974; Ohmi et al., 1976). Experimental investigations require expensive measurement devices and excessive number of measurement runs caused by the high number of characteristic parameters such as frequency, amplitude, and Reynolds number (Richardson, 1928; Richardson and Tyler, 1930; Atabek et al., 1965; Linford and Ryan, 1965; Florio and Mueller, 1968, Harris et al., 1969; Denison, 1970; Denison et al., 1971; Gerrard and Hughes, 1971; Hino et al., 1976; Muto and Nakane, 1980; Ohmi et al., 1982; Unsal et al., 2005). Numerical exact solutions of the momentum equations based on finite-difference technique are somewhat more common for Newtonian fluids, but the constitutive complexities of non-Newtonian fluids hinder even these powerful techniques (Rosenhead, 1963; Gerlach and Parker, 1967; Balmer and Fiorina, 1980; Donovan et al., 1991). Computational models based on finite-volume technique have recently accepted as a vital means for investigating the pulsatile blood flow especially in complex regions (Steinman, 2002; Jung et al., 2006). Computational studies may not have the disadvantages of experimental studies, but there are other difficulties to be handled such as the mathematical complexity of pulsatile flow dynamics, the requirement for an excessive number of finite elements to obtain accurate solutions, and the application of realistic boundary conditions without simplifications. Developing an efficient and reliable CFD (Computational Fluid Dynamics) model is thus a hard task. Moreover, CFD models should be validated by accurately chosen and treated experimental data. For nearly three decades, CFD models have, however, been used by investigators to address pulsatile blood flow because of their advantage in the simplicity of handling a variety of pulatile flow conditions by only changing related initial and boundary conditions, as well as the possibility of providing information that is hard or even impossible to measure. CFD models have been found to be an efficient and reliable tool during this development period. It is likely to continue to play an important role in pulsatile flow studies.

It has been understand from the above literature that the flow field of laminar pulsatile pipe flow is dependent on the dimensionless frequency parameter, $\sqrt{\omega'}$ (i.e., Strouhal number or Womersley parameter) but not on Reynolds number and amplitude (Ohmi et al., 1976). The laminar regime of pulsatile pipe flow can be classified into three sub-regions such as quasi-steady, intermediate and inertia dominant ones with respect to this frequency parameter. The limiting values of the frequency parameter were evaluated respectively as $\sqrt{\omega'_q}$ =1.32 between the quasi-steady and the intermediate regions, and as $\sqrt{\omega'_t}$ =28.0 between the intermediate and the inertia dominant regions (Ohmi et al., 1981a). At low frequencies (i.e., $\sqrt{\omega'} < 1.32$), the cross sectional distribution profile of axial velocity is parabolic so that the flow is in quasi-

steady state. At high frequencies (i.e., $\sqrt{\omega'} > 1.32$), the interaction between viscous and inertial effects alters the axial velocity profile of oscillatory and pulsatile pipe flows so that it gradually varies from parabolic shape to a rectangular-like shape with an increase in $\sqrt{\omega'}$ up to 5.0 and so it has a peak. The peak of distribution tends to approach the pipe wall gradually with further increases in $\sqrt{\omega'} > 5.0$ (Hino et al., 1976; Muto and Nakane, 1980; Ohmi et al., 1982). In the literature, there exists an indistinctness about the variation mechanism of the parabolic profile up to a rectangular-like shape and the movement of the distribution peak towards the pipe wall when the value of $\sqrt{\omega'}$ increases over 5.0 in the intermediate region. The unique variation mechanism proposed for it is the gradual variation by Muto and Nakane (1980) due only flow visualizations. It has also been understand from the above literature that the results of analytical, approximate, and experimental investigations on the velocity profile in the quasi-steady region of laminar regime confirms each other within a deviation range of 5%, but this deviation increases with the increase of $\sqrt{\omega'}$ in the intermediate region. However there has no any finite-difference and/or finite-volume technique based computational study on the velocity field in the intermediate region of laminar-pulsatile pipe flow. The limited numbers of the present computational studies are only directed on the variation of velocity profile as a function of the power-law index of fluid viscosity (Balmer and Fiorina, 1980) and on the flow resistance as a function of $\sqrt{\omega'}$ (Donovan et al., 1994).

In view of the literature, the present study is directed to clarify the indistinctness about the variation mechanism of the velocity profile throughout the intermediate region of laminar-pulsatile pipe flow by means of both the experimental and the computational techniques in order to evaluate a comparison basis between them. In the first part of this study, the velocity profiles across the cross-section of a horizontal smooth pipe at a test section and the static pressure differences between two static taps symmetrically apart from the test section are measured through 30 different instants of a pulsation cycle by means of traversing a hot-wire probe and a pressure transducer respectively for 29 different experimental runs covering the ranges; $2.26\text{x}10^3 \pm 17\% \leq Re_{ta} \leq 4.36\text{x}10^3 \pm 10\%$, $5.1 \pm 4\% \leq \sqrt{\omega'} \leq 28.0 \pm 0.05\%$, $0.03 \leq A_1 \leq 0.71$. In the second part, the variation of velocity profiles are also analyzed computationally by using the finite-volume based Fluent software-package v6.3.26 for the initial and the boundary conditions selected to be same with four different ones of the experimental runs. Finally, the experimental and the computational velocity profiles evaluated in the present study are compared with each other and with the well-known Blasius's and Prandtl's distributions for the laminar and the turbulent regimes of the steady pipe flow respectively. As a consequence of these comparisons, evaluated results on the variation of velocity profiles with respect to the characteristic flow parameters; $\sqrt{\omega'}$, Re_{ta}, A_1 and the results on the compatibility of computational technique for this flow type are discussed in view of the citations in the available literature (Hino et al., 1976; Muto and Nakane, 1980; Ohmi et al., 1976, 1981a, 1982).

EXPERIMENTAL STUDY

Experimental study is carried out on a specially constructed test rig to determine the characteristics of pulsatile pipe flow at different flow regimes. A schematic layout of the test rig is shown in Fig. 1. Air at ambient conditions is used in the test rig as the working fluid. The test rig is made up of the basic components; namely, steady flow generation unit, pulse generator, pipe line, flow regulation unit, measurement instruments, and an interactive data acquisition and control system. The pipe line is constructed of rigid and smooth polyvinyl chloride pipe with 50.4 mm internal diameter to enable velocity and pressure drop measurements. The pipe line is connected to the turbulence removing unit at one end and to the piston of the pulse generator at the other end by means of two bell-shaped smooth transitions. The cross-sectional areas of the transitions are designed to change steadily in the flow direction, so that the mean velocity of air changed steadily through the transitions. A honeycomb made of plastic straws preceded by a coarse screen and followed by a fine screen is used in the flow regulation unit at the air entry of the pipe line to control scale and intensity of flow turbulence in view of the investigations by Loehrke and Nagib (1976), and Farell and Youssef (1996). The operation performance of the rig is made fairly well by means of conducting a series of preliminary calibration tests based on pressure drop and velocity measurements for generated pulsatile flows with different frequency, amplitude and Reynolds numbers. The time-averaged (mean) and the oscillatory components of the pulsatile flow are generated by means of a centrifugal suction fan and a reciprocating piston driven by the slider crank of a scotch-yoke mechanism, respectively. The magnitude of the mean flow component is controlled by controlling the rotational speed of the fan by means of an AC motor speed control unit (6SE3221-3DC40, SIEMENS). The time-averaged Reynolds number, Re_{ta} of the generated pulsatile flow can thus be settled to any chosen value by adjusting the rotational speed of the fan. Pulsation frequency is controlled by adjusting the rotational speed of the slider crank by means of a second AC motor speed control unit (6SE3013-4BA00, SIEMENS). Pulsation amplitude can only be adjusted by changing the stroke of piston.

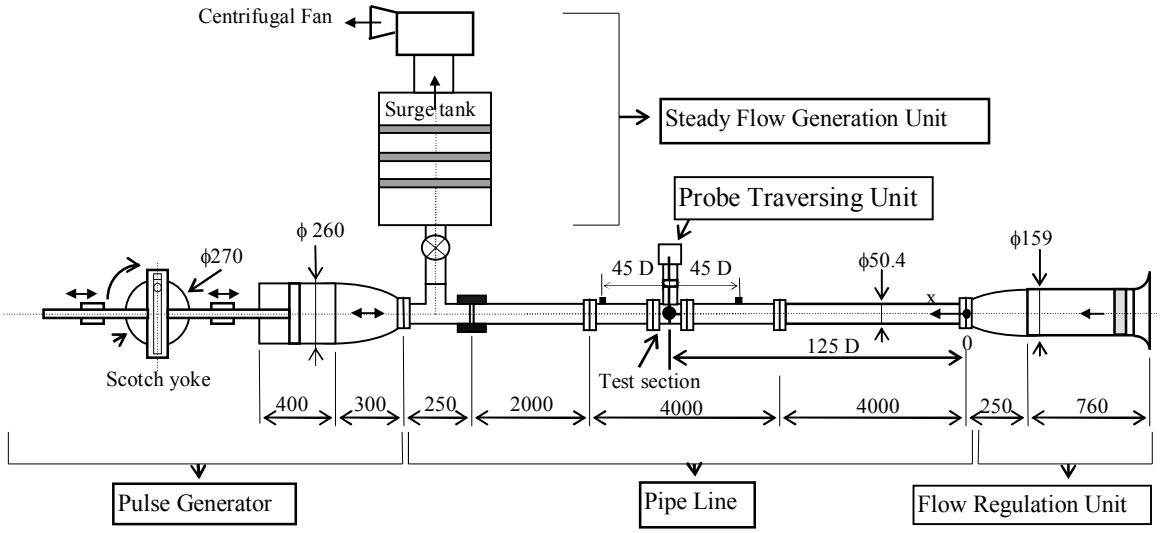

Figure 1. A schematic layout of the test rig.

Velocity measurements are made at the test section by using a hot-wire anemometer (CTA 56C01, DANTEC) in combination with the 55P11 general purpose type miniature hot-wire probe. The test section is located 125 D downstream of the flow regulation unit to obtain the fully developed laminar-pulsatile pipe flows in view of the studies of Florio and Mueller (1968), and Ohmi et al. (1976). The local axial velocity, u is measured at 14 different radial positions to obtain the velocity profile across the pipe cross section. The measurement sensitivity of u with the how-wire anemometer changes respectively from ±2% to ±0.5% when it changes from 0.15 m/s to 3 m/s in the present study. The hot-wire probe traversing mechanism used for this purpose is driven by a computer-controlled step motor with 200 steps per revolution. The step motor had a step rate of 1.8^0/digital signal pulse. The traversing mechanism transforms rotational motion of the step motor into a linear displacement sensed by a micrometer with a dimensional sensitivity of ±2.5 micrometers. The static pressure difference between two static taps symmetrically apart from the test section with 45D axial distance is measured by using a difference type inductive pressure transducer (PD1, HBM) with a diaphragm of 300 Hz natural frequency. It has a measurement range of 0 to ±0.01bar. The HBM's 4.8 kHz carrier frequency type amplifier, MVD 2555 was also used in connection with the pressure transducer. The measurement sensitivity of ΔP changes respectively from ±5% to ±0.5% when it changes from 0.3 Pa to 5 Pa in the present study. The determination of the axial apart distance (L=90D) between the taps is done in view of the study carried by Zhao et al. (1990). The fully developed static pressure gradient dP/dx at the test section of the pipe line is then approximated by ΔP/L with accuracies better than 99%.

The period, T of a pulsation cycle changes with changing the pulsation frequency. So it should be made dimensionless to obtain a common comparison basis between the measurements for different pulsation periods. The non-dimensional phase parameter is used for this purpose as mostly used in literature; phase number= ω.t /(2π/30), where t is the time in seconds changes in the range $0 \le t \le T$ through the cycle and ω is the angular frequency of the pulsation in radian/seconds. The axial velocity data at 14 radial positions across the pipe and the static pressure difference data for any experimental case are accumulated at 30 different but equally spaced instants of a pulsation cycle. This timing of the data accumulation is obtained by means of the triggering time signals generated by an optical encoder (TRD-J-30-RZV, Koyo Electronics) coupled on the crank of the pulse generator. The data accumulation for each of 30 different phases in a cycle is continued through 200 cycles to obtain the data amounts allowing the treatment of an ensemble averaging. Control of the probe traversing unit of the hot-wire anemometer and all accumulation, acquisition, and processing of the measured velocity and pressure difference data in the test rig are carried by means of a fully computer-aided interactive data acquisition and control system. More detailed descriptions of the test rig, the data acquisition system, and the experimental error analysis can be found in our previous studies Carpinlioglu and Gundogdu (2001b) and Gundogdu and Carpinlioglu (2002).

The velocity and pressure difference measurements of this study were planned for 50 different systematically organized runs of the test rig with 2 different time-averaged Reynolds number, Re_{ta} of $2.26x10^3$±17% and $4.36x10^3$±10%, 5 different dimensionless frequency parameter, $\sqrt{\omega'}$ of 5.1±4%, 7.09±0.6%, 12.5±0.2%, 23.0±0.1%, and 28.0±0.05%, and 5 different piston strokes of 20 mm, 40 mm, 70 mm, 100 mm and 130 mm. The preliminary calibration measurements however indicated that the generated pulsatile pipe flows for 21 of the planned runs are partly or fully reversed for which the present direction-insensitive hot-wire probe can not be used (Gundogdu, 2000). The detailed velocity and pressure difference measurements

are therefore conducted for the remaining 29 different runs listed in Table 1 as covering the intermediate region of the laminar-pulsatile pipe flow.

Table 1. Characteristic parameters of the experimental runs.

Run No	Re_{ta}	A_1	$\sqrt{\omega'}$	Stroke (mm)
1	1869.0	0.0582	4.899	20
2	1924.6	0.0790	7.110	
3*	**2062.6**	**0.1572**	**12.516**	
4	1901.1	0.5517	23.035	
5	2077.6	0.7113	28.001	
6	4346.6	0.0333	4.926	
7	4201.4	0.0595	7.114	
8	4131.0	0.0939	12.509	
9	4229.3	0.2733	23.035	
10	4126.6	0.4271	28.015	
11	2057.3	0.1311	5.287	40
12	2125.8	0.1634	7.088	
13	2075.3	0.4085	12.495	
14	4064.6	0.1061	5.312	
15*	**4613.2**	**0.1310**	**7.079**	
16	4210.1	0.2285	12.484	
17	2621.5	0.1903	5.312	70
18	2553.4	0.2432	7.082	
19	4786.2	0.1445	5.287	
20	3927.3	0.2391	7.082	
21	3990.7	0.4171	12.527	
22	2653.9	0.2632	5.262	100
23	1924.9	0.4793	7.079	
24	4298.9	0.1952	5.005	
25	4163.5	0.3239	7.105	
26*	**2233.0**	**0.4043**	**5.153**	130
27	1964.8	0.6449	7.129	
28*	**4240.0**	**0.2822**	**5.084**	
29	4032.8	0.4466	7.121	

*denotes the computationally analyzed runs

COMPUTATIONAL STUDY

The horizontal pipe line of the experimental test rig together with the flow regulation unit at the air entry (see Fig.1) is considered as a 2-Dimensional axis-symmetric tubular system in order to reduce the number of grids and created by using the Gambit v2.4.6 software. The honeycomb, the coarse screen, and the fine screen present in the flow regulation unit of the test rig is not considered in the inlet section of the computational tubular domain for this study according to the requirement on excessive number of 3-Dimensional grids and so extremely long solution and convergence times, but it must be noted here as a further work to evaluate absolute similarity between the experimental and the computational domains. The mirror view of the axis-symmetric geometry combined with the structured mesh of computational domain for a main flow along the x-axis is shown schematically in Fig. 2.

A commercial CFD software package, Fluent v6.3.26 is used to model the laminar-pulsatile viscous pipe flow. Governing equations of mass and momentum with appropriate initial and boundary conditions are adopted to solve numerically everywhere in the system. The continuity and momentum equations for 2D incompressible flows can be written respectively as follows:

$$\frac{\partial \rho}{\partial t} + \rho_0 \left(\frac{\partial u}{\partial x} + \frac{\partial v}{\partial r} + \frac{v}{r} \right) = 0 \tag{1}$$

$$\frac{\partial u}{\partial t} + u\frac{\partial u}{\partial x} + v\frac{\partial u}{\partial r} = -\frac{1}{\rho_0}\frac{\partial P}{\partial x} + \upsilon\left(\frac{\partial^2 u}{\partial x^2} + \frac{\partial^2 u}{\partial r^2} + \frac{1}{r}\frac{\partial u}{\partial r} \right) + \frac{\upsilon}{3}\frac{\partial}{\partial x}\left(\frac{\partial u}{\partial x} + \frac{\partial v}{\partial r} + \frac{v}{r} \right) \tag{2}$$

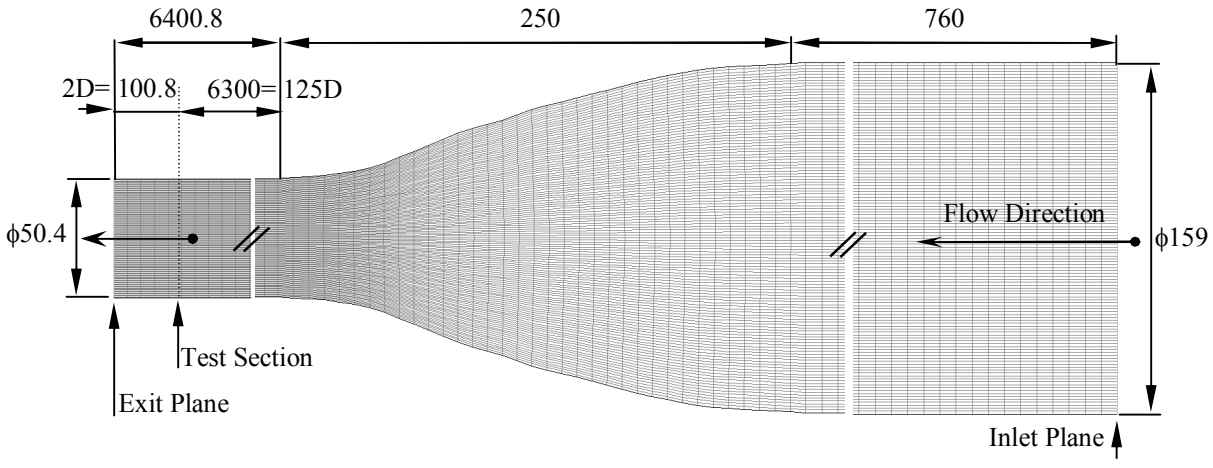

Figure 2. A mirror view of 2D axis-symmetric mesh of the computational domain.

$$\frac{\partial v}{\partial t}+u\frac{\partial v}{\partial x}+v\frac{\partial v}{\partial r}= -\frac{1}{\rho_0}\frac{\partial P}{\partial r}+\upsilon\left(\frac{\partial^2 v}{\partial x^2}+\frac{\partial^2 v}{\partial r^2}+\frac{1}{r}\frac{\partial v}{\partial r}-\frac{v}{r^2}\right) +\frac{\upsilon}{3}\frac{\partial}{\partial x}\left(\frac{\partial u}{\partial x}+\frac{\partial v}{\partial r}+\frac{v}{r}\right) \quad (3)$$

where x is the axial coordinate, r is the radial coordinate, P is the static pressure, u is the axial velocity, v is the radial velocity, ρ_0 is the density at t=0, υ is the kinematic viscosity. For pulsatile flow, an ensemble-averaged (i.e., short-time averaged) value has also a long-time averaged value and an oscillatory component due to the pulsation which are denoted by subscripts "ta" and "os" respectively. The instantaneous values can so be written as; $P=\overline{P}_{ta}+\overline{P}_{os}$; $u=\overline{u}_{ta}+\overline{u}_{os}$; $v=\overline{v}_{ta}+\overline{v}_{os}$. At the test section of the test rig, the values of cross sectional mean velocity, U_m predicted from the previously measured velocity distributions through the 30 different phases of the pulsation cycle for the selected four different runs; Run 28, Run 26, Run 15, and Run 3 as marked by the star (*) on Table 1 are therefore fitted with Fourier series up to sixth harmonics as follow;

$$\overline{U}_m=\overline{U}_{m,ta}+\sum_{n=1}^{6}\left|\overline{U}_{m,os,n}\right|\cos(n\omega t+\angle\overline{U}_{m,os,n}) \quad (4)$$

and thus, the time-averaged value $\overline{U}_{m,ta}$, the amplitude $\left|\overline{U}_{m,os,1}\right|$, and the phase angle $\angle\overline{U}_{m,os,1}$ of the fundamental wave are determined for each of the runs as follows;

$$\overline{U}_m=\overline{U}_{m,ta}+\left|\overline{U}_{m,os,1}\right|\cos(\omega t+\angle\overline{U}_{m,os,1}) \quad (5)$$

It is well known that the general tradition in CFD packages is applying the pressure boundary condition at the exit plane and the velocity boundary condition at the inlet plane. However, the application of the reverse of this tradition can also be possible under some circumstances as suggested by the Introductory Fluent Notes (Ansys Inc., 2006). Although the time-dependent variation of static pressure at the test section is not measured, the cross sectional velocity distribution at the test section and the static pressure difference around it are both measured previously throughout the pulsation cycles in the first part of the present study. Instead of using the general tradition about the boundary conditions, the velocity outlet and the pressure inlet boundary conditions are therefore preferred as a necessity in the computational part of the present study. The first harmonic of the U_m wave predicted from Eq. 5 is used to define the cross sectional mean velocity at the exit plane of the tubular computational domain shown in Fig. 2 as a "velocity outlet" boundary condition by specifying negative velocity as enabled by the Fluent software. This time-dependent velocity outlet condition at the exit plane is defined into the Fluent by means of a user defined function, UDF in C++ language as an interpretation. The pressure inlet boundary condition is applied at the inlet plane of the flow regulation unit of the domain by means of setting it to the atmospheric pressure. In order to eliminate the exit effects on the flow at the test section, the exit plane of the tubular domain is located at 100.8 mm (i.e., 2D) downstream of the test section as a straight buffer zone. The no-slip condition is imposed at the pipe walls.

Once the appropriate continuum structures have been defined, the pressure-based segregated algorithm with an implicit unsteady second order scheme is used together with non-iterative time advancement (NITA) option under transient controls to solve the governing equations. The momentum equations are discretized using a second order upwind discretization scheme. The pressure term is firstly discretized using a second order scheme and then both the pressure and the velocity terms are coupled with each other by using the Pressure-Implicit with Splitting of Operators (PISO) scheme. Evaluating grid independent solutions is also an important aspect to minimize the error in CFD results. So, it is practical to reach the grid independent solutions by means of several tests on computational mesh. The number of cell elements and the number of nodes in the half of the entire fluid domain are received respectively as 68100 and 69296 for the initial test of computational mesh. They are also checked respectively for the 17040 and 17639 numbers through the secondary test. Fig. 3 shows the results on the pressure difference at the test section after six complete pulsation cycles for these two different tests of computational mesh. It is seen from the figure that the pressure difference data for the both tests of mesh are quite similar through the all 30 phases of the cycle. This indicates that the 68100 cells are enough to reach the grid independency for the solutions and therefore the test for a greater number of cells is not required. To ensure proper temporal resolution, transient calculations are conducted by using 900 and 1800 equal time steps per cycle. Additionally, calculations are continued for the six complete pulsation cycles to ensure that cycle-to-cycle variations of pulsation become minimal.

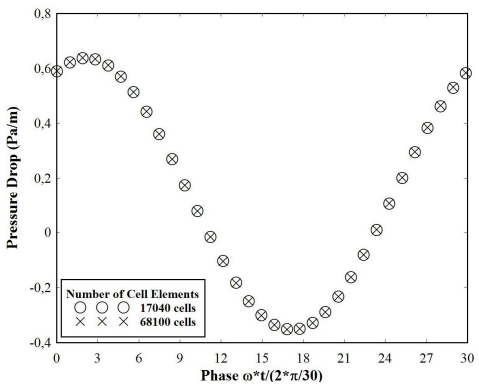

Figure 3. Results of ΔP/L computation for two different cell numbers.

The computational study is conducted repetitively for the four conditions kept to be same with the conditions of the

selected four different experimental runs; namely, Run 28, Run 26, Run 15, and Run 3 with different characteristic flow parameters; Re_{ta}, $\sqrt{\omega'}$, and A_1. The experimental U_m data at the test section are ready for these runs to use as benchmarks for the computational study. These runs are selected to be typical examples for the intermediate region of laminar-pulsatile pipe flow (see Table 1). The availability of the fully-developed velocity profiles at the test section is also checked as proper before each of the computational runs. The time-dependent variations of both the cross sectional velocity profiles and the pressure difference at the test section are then received for these runs as an output of the computational study and compared with the corresponding experimental data.

RESULTS AND DISCUSSION

In the first part of this study, the variations of the cross sectional mean velocity, U_m and the approximate pressure gradient, $\Delta P/L$ through 30 different instants (phases) of a pulsation cycle are evaluated due to the velocity distribution and the pressure difference measurements for the 29 different runs listed in Table 1. In the second part, the variation of the pressure gradient, $\Delta P/L$ is also computed numerically by means of using model fits on the experimentally evaluated variation of the cross sectional mean velocity as an input parameter at the exit plane of test section to the Fluent for the Run 28, Run 26, Run 15, and Run 3. The variations of the experimentally evaluated U_m and $\Delta P/L$ data, the model fit on U_m data, and the computational output data on $\Delta P/L$ through a pulsation cycle are all shown in Figs. 4a-4d for these four runs. The coefficient of determination, R^2 and the standard error of estimate are used together with the statistical models to determine and show the relationship between the measured data and the model fits on U_m. The deviations of the model fits from a standard sine wave are therefore shown in Table 2 for these runs.

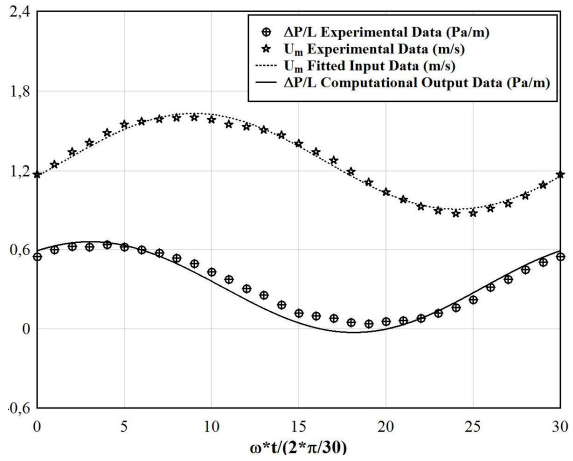

(a) Run 28: Re_{ta}=4240.0, A_1=0.2822, $\sqrt{\omega'}$ =5.084

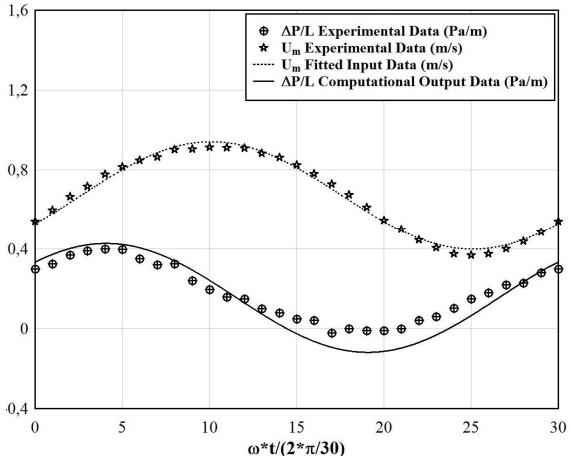

(b) Run 26: Re_{ta}=2233.0, A_1=0.4043, $\sqrt{\omega'}$ =5.153

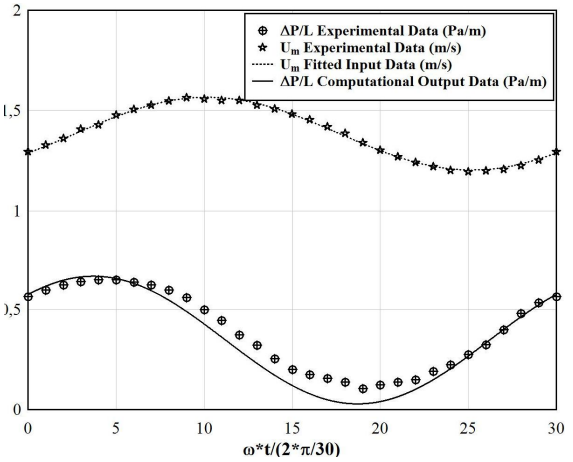

(c) Run 15: Re_{ta}=4613.2, A_1=0.1310, $\sqrt{\omega'}$ =7.079

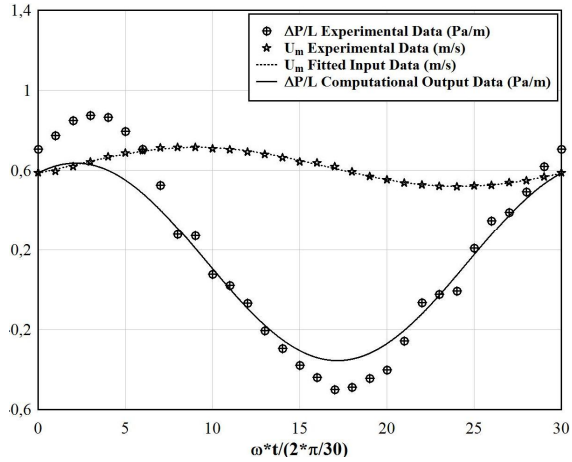

(d) Run 3: Re_{ta}=2062.6, A_1=0.1572, $\sqrt{\omega'}$ =12.516

Figure 4. Variations of experimental and computational U_m and $\Delta P/L$ through a pulsation cycle for Run 28, Run 26, Run 15, and Run 3 respectively.

Table 2. Statistics between the measured data and the model fits on U_m.

Run No	R^2	Standard error
Run 28	0.9886	0.0274
Run 26	0.9894	0.0201
Run 15	0.9972	0.0068
Run 3	0.9952	0.0048

It is seen from the Figs. 4a-4d that; the dimensionless phase (i.e., $\omega t/(2\pi/30)$) intervals, 0~10 and 25~30 approximately show the accelerating period of the pulsation cycle where the experimental values of $dU_m/dt > 0$. However, the phase interval, 10~25 shows the decelerating period where $dU_m/dt < 0$ for all of the studied runs. The pressure gradient, $\Delta P/L$ reaches a maximum near the middle-inflection phase (~3) of accelerating period and reaches a minimum near the middle-inflection phase (~18) of decelerating period. The phase lags of the U_m and the $\Delta P/L$ waves from the generated pulsation at the downstream pulse generator are approximately 120° and 42°-48° respectively and so the phase shift angles between them are detected to be varying between 72° and 78° for these four runs. As the $\sqrt{\omega'}$ increases, the phase shift increases slightly. The computational output data on $\Delta P/L$ show a good agreement with the corresponding experimental ones for nearly all phases of these runs except the phases near the inflection points of accelerating and decelerating periods (see especially Fig. 4d). The bad agreement near the inflection points becomes better when $\sqrt{\omega'}$ decreases and Re_{ta} increases.

In order to show clearly the absolute deviations between the measured and the computed axial velocity data, the measured and numerically computed radial profiles of axial velocity, u at 10 different phases of a pulsation cycle are also shown in Figs. 5a through 5d for these four runs, respectively. In these figures; the experimental and the computed velocity profiles are shown by means of different data symbols and solid lines respectively for the selected 10 different phases; 0(or 30), 3, 6, 9, 12, 15, 18, 21, 24, 27 through the pulsation cycle. These ten phases are especially selected to be equally spaced in order to fully represent the variation of velocity profiles through the accelerating (0(or 30), 3, 6, 9, 27) and the decelerating (12, 15, 18, 21, 24) periods including their middle-inflection phases (3 and 18). These figures show that; the computational and experimental data on axial velocity confirm each other except the near-wall region for $0.95<r/R<1.0$ and the central core region for $r/R<0.4$ at all phases of the runs. The deviation in the near-wall region seems to be caused by the well-known wall-proximity effect on the hot-wire probe used for the velocity measurement. However in the core regions, the computed data considerably underestimate the corresponding experimental ones and the percent deviation between them reaches to a maximum at the centerline(r/R=0). The detected maximum deviations at the centerline become 10.5 % for Run 28, 13.5 % for Run 26, 9.1 % for Run 15, 1.7 % for Run 3 at different phases. It can be detected that the percent deviation in the core region directly proportional with A_1 but indirectly proportional with both of $\sqrt{\omega'}$ and Re_{ta}. It decreases when A_1 decreases but when $\sqrt{\omega'}$ and Re_{ta} increase. It can be also understand that $\sqrt{\omega'}$ and A_1 parameters seem to be more effective than Re_{ta} on the deviation.

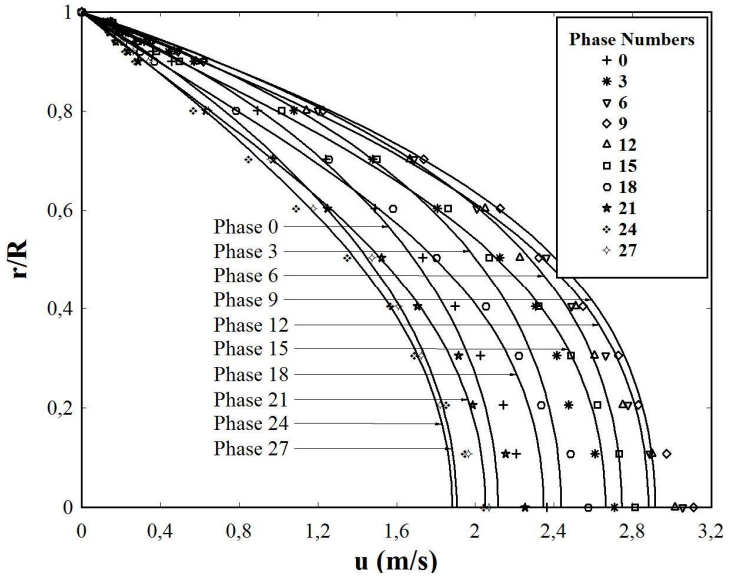

Fig. 5(a) Run 28: Re_{ta}=4240.0, A_1=0.2822, $\sqrt{\omega'}$ =5.084

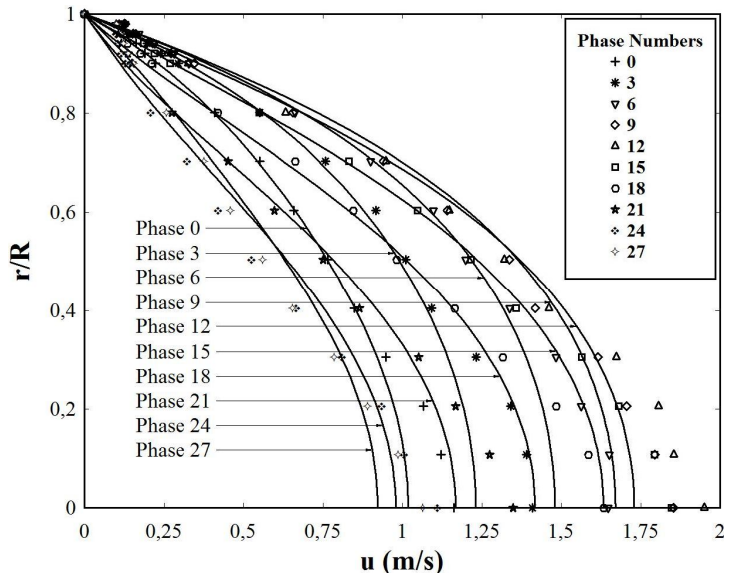

Fig. 5(b) Run 26: Re_{ta}=2233.0, A_1=0.4043, $\sqrt{\omega'}$ =5.15

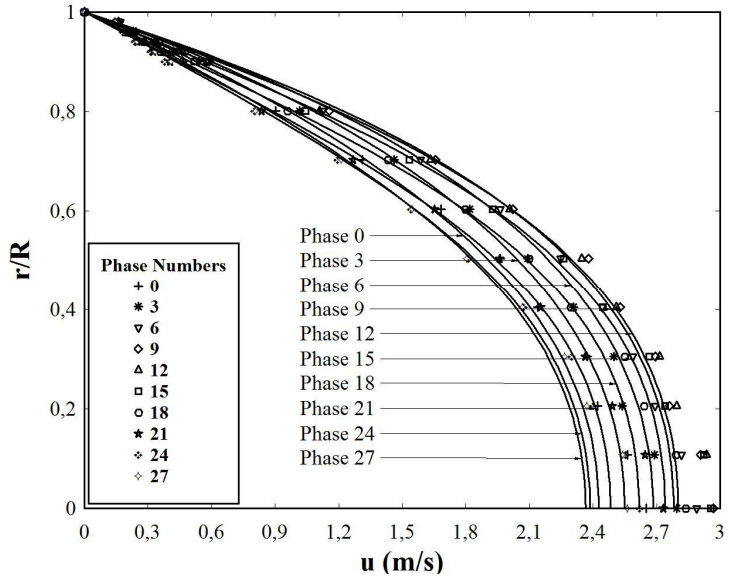

Fig. 5(c) Run 15: Re_{ta}=4613.2, A_1=0.1310, $\sqrt{\omega'}$ =7.079

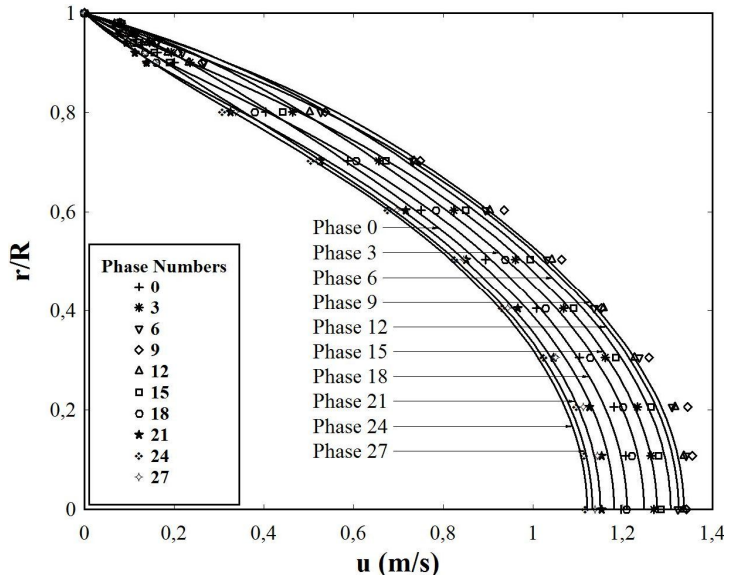

Fig. 5(d) Run 3: Re_{ta}=2062.6, A_1=0.1572, $\sqrt{\omega'}$ =12.516

Figure 5. Variations of measured and computed velocity profiles with r/R at different phases for Run 28, Run 26, Run 15, and Run 3 respectively.

For better understanding the reasons of this deviation between the experimental and the computed velocity data especially in the central core region and comparing them with the well-known Blasius's parabolic and the Prandtl's rectangular-like (i.e., blunt) shaped velocity profiles corresponding to the steady laminar and the steady turbulent pipe flows respectively, Figs. 6a through 6d are formed by means of making non-dimensional the lower axes of Figs. 5a-5d. Additionally, Figs. 6e and 6f are also drawn for the only experimentally studied runs; Run 9 and Run 10 respectively. In these figures; the dimensionless velocity data, u/U_{cl} for both the experimental and the computational studies are plotted with respect to the dimensionless radius, r/R and labeled with different symbols and dotted lines respectively together with the corresponding phase indexes. Both the Blasius's parabolic velocity profile and the Prandtl's $1/7^{th}$-power law velocity profile are also represented with the solid and the centered lines respectively. It is seen from Figs. 6a-6f that the tendency of numerically computed velocity profiles is slightly blunter than the tendency of the corresponding experimental velocity profiles for the all phases. This inconsistency between the tendencies has an order greater than the experimental error ranges of the used hot-wire anemometer system and it can be caused mainly by the preferred 2D-mesh of the tubular domain instead of using the realistic but complex 3D-mesh in the computational part of this study. Especially the turbulence removing unit that includes a honeycomb, a coarse screen, and a fine screen at the air entry of the experimental set-up should be well adapted to the numerical computation by means of a 3D-mesh of domain in a further study. Against the mentioned inconsistency, there are some critical consistent results observed as that; both the experimental and the computed velocity profiles reach to the sharpest profile (i.e., triangular-like) at the end of decelerating period or at the start of accelerating period (i.e., ~25^{th} phase (see Figs. 4a-4d)). Both of them become gradually blunter through the all accelerating period (i.e., between the phases; 25-30(0)-10) and almost reach to the most blunt one at the end of accelerating period (i.e., ~10^{th} phase). After that both of them become gradually sharper through the all decelerating period (i.e., between the phases; 10-25) and return to the sharpest profile at the end of decelerating period (i.e., ~25^{th} phase).

It can be also seen from Figs. 6a-6f that; the general tendencies of both the experimental and the computational velocity profiles are very similar to the Blasius's distribution but differ appreciably from the Prandtl's distribution for the all six runs that are so truly considered as typical runs of the laminar-pulsatile pipe flow. Both the experimental and the computational velocity profiles become blunter than the Blasius's distribution in some phases of the pulsation cycle but become sharper than it in the remaining phases for the all runs. When $\sqrt{\omega'}$ increases over ~5.0 up to ~28.0; the sharper profiles approach to the Blasius's distribution but the blunter profiles drop below or underestimate it at the central core region (i.e., $r/R<0.4$) and move up to the wall in the outer region (i.e., $0.6<r/R<1.0$). As can be seen especially from Figs. 6e and 6f for the $\sqrt{\omega'}$ values of ~23.0 and ~28.0, the experimental velocity profiles for the phases 6 and 9 in the second half of the accelerating period and for the phases 12 and 15 in the first half of the decelerating period approach quite close of the wall in the outer region and show almost a peak of rectangular-like velocity profile at $r/R\approx0.85$ when $\sqrt{\omega'} \approx 28.0$.

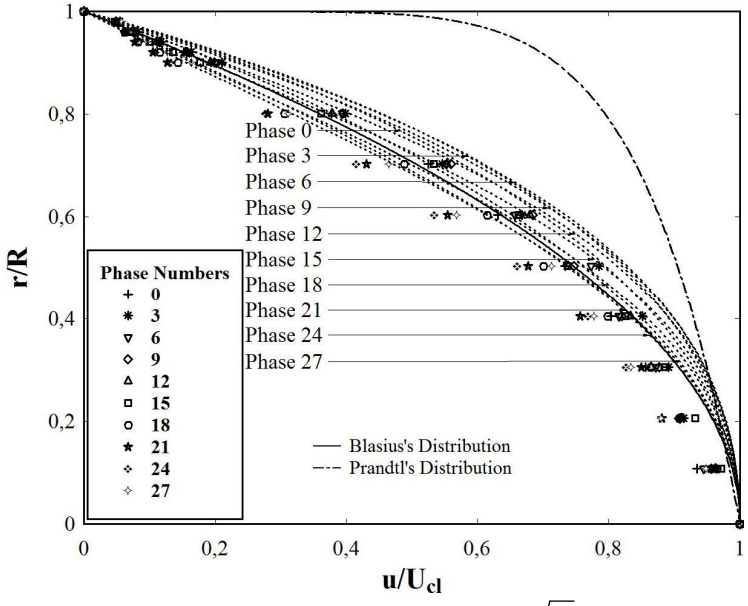

Fig. 6(a) Run 28: Re_{ta}=4240.0, A_1=0.2822, $\sqrt{\omega'}$ =5.08

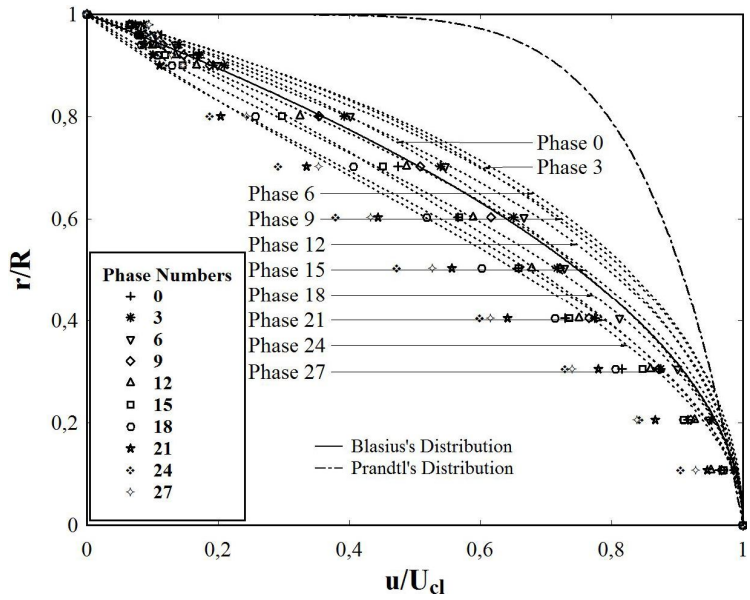

Fig. 6(b) Run 26: Re_{ta}=2233.0, A_l=0.4043, $\sqrt{\omega'}$ =5.153

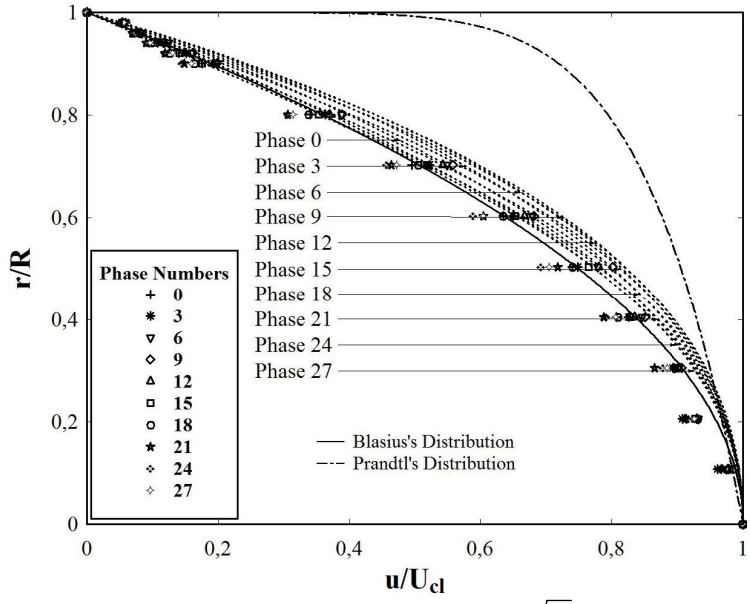

Fig. 6(c) Run 15: Re_{ta}=4613.2, A_l=0.1310, $\sqrt{\omega'}$ =7.079

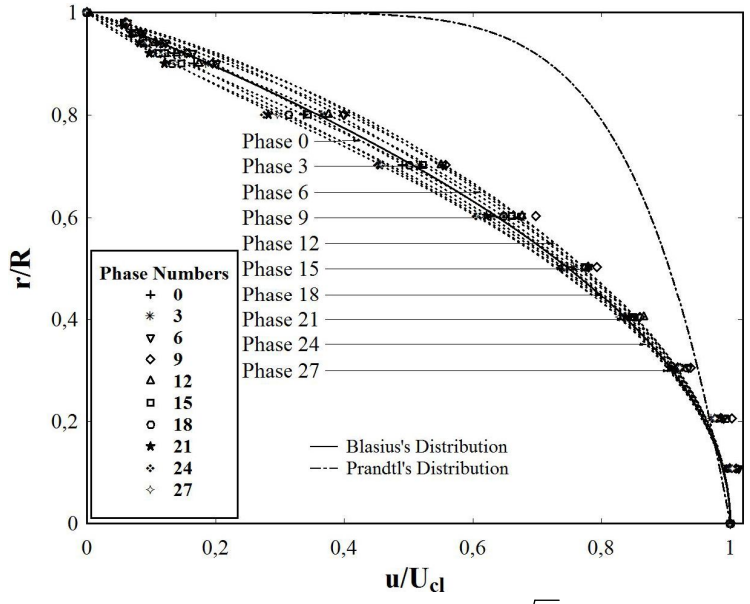

Fig. 6(d) Run 3: Re_{ta}=2062.6, A_l=0.1572, $\sqrt{\omega'}$ =12.516

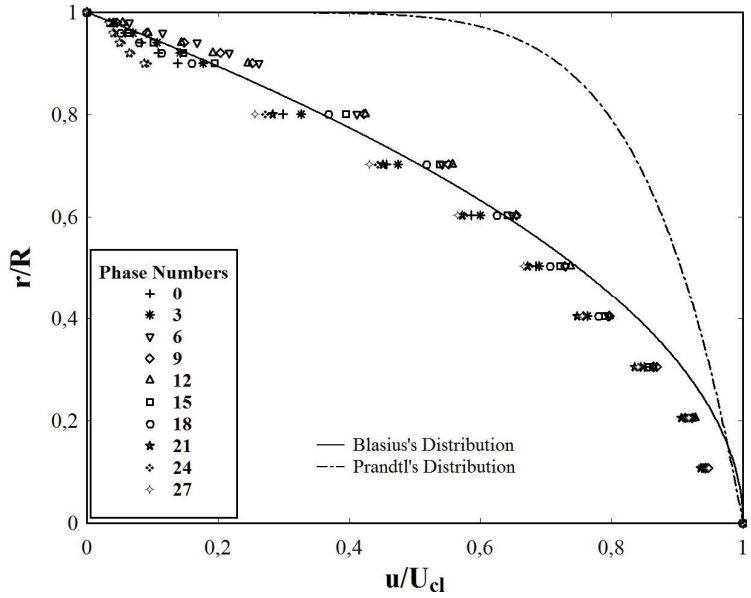

Fig. 6(e) Run 9: Re_{ta}=4229.3, A_1=0.2733, $\sqrt{\omega'}$ =23.035

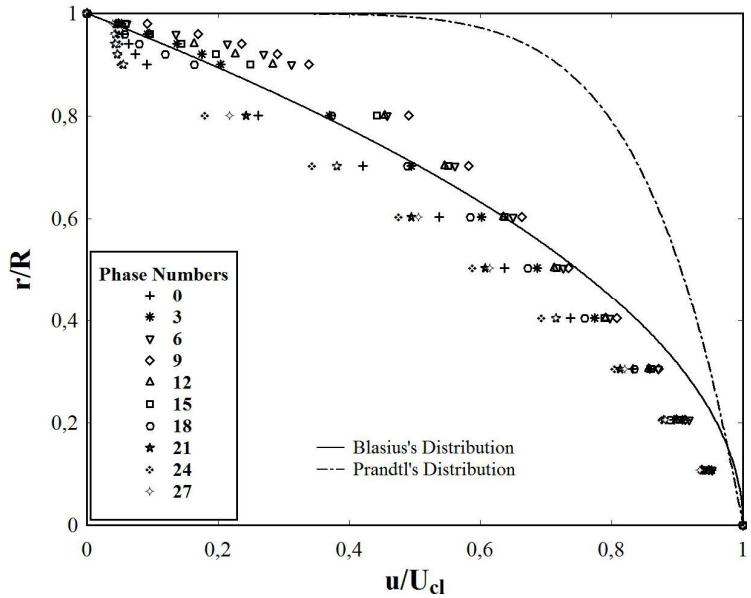

Fig. 6(f) Run 10: Re_{ta}=4126.6, A_1=0.4271, $\sqrt{\omega'}$ =28.015

Figure 6. Variations of measured and computed dimensionless velocity, u/U_{cl} with r/R at different phases for Run 28, Run 26, Run 15, Run 3, Run 9, and Run 10 respectively.

This fact of the experimental and the computational velocity profiles in the present study show that; the limiting value of the dimensionless frequency parameter between the intermediate and the inertia dominant regions of the laminar-pulsatile pipe flow can be accepted as $\sqrt{\omega'_t}$ ≈28.0 proposed firstly by Ohmi et al. (1981a) and the peak of the velocity profile tends to gradually approach the pipe wall when $\sqrt{\omega'}$ increases from ~5.0 to the upper limit, ~28.0 of the intermediate region as addressed initially by Muto and Nakane (1980) due only flow visualizations.

CONCLUSIONS

The velocity field of fully developed laminar-pulsatile pipe flow in the intermediate region is investigated systematically by means of the experimental and the computational studies. It can be concluded from these studies that:

1. The phase shift angles between the measured U_m and $\Delta P/L$ pulsation waves increases slightly when $\sqrt{\omega'}$ increases.
2. The computed $\Delta P/L$ data show a good agreement with the corresponding experimental ones for nearly all

phases of pulsation in the intermediate laminar region except the phases near the middle-inflection points of accelerating and decelerating periods. The bad agreement near the inflection points decreases when $\sqrt{\omega'}$ decreases and Re_{ta} increases.

3. The computational and experimental data on axial velocity confirm each other except the near-wall region for $0.95<r/R<1.0$ and the central core region for $r/R<0.4$ at all phases of the runs. The deviation in the near-wall region seems to be caused by the well-known wall-proximity effect on the hot-wire probe used for the velocity measurement. However in the core regions, the computed data considerably underestimate the corresponding experimental ones and the percent deviation between them reaches to a maximum at the centerline(r/R=0). It can be also detected that the percent deviation in the core region directly proportional with A_1 but indirectly proportional with both of $\sqrt{\omega'}$ and Re_{ta}. It decreases when A_1 decreases but when $\sqrt{\omega'}$ and Re_{ta} increase. It can be also understand that $\sqrt{\omega'}$ and A_1 parameters seem to be more effective than Re_{ta} on the deviation.

4. The tendency of numerically computed velocity profiles is also slightly blunter than the tendency of the corresponding experimental velocity profiles for the all phases. This inconsistency between the tendencies has an order greater than the experimental error ranges of the used hot-wire anemometer system and it can be caused mainly by the used 2D-mesh of domain in the computational part of this study. Especially the flow regulation unit at the air entry of the experimental set-up should be well adapted to the computational study by means of a 3D-mesh of the tubular domain in a further study.

5. The general tendencies of both the experimental and the computational dimensionless velocity profiles are very similar to the Blasius's distribution but differ appreciably from the Prandtl's distribution for the all runs in the intermediate region of the laminar-pulsatile pipe flow. Both the experimental and the computational dimensionless velocity profiles become blunter than the Blasius's distribution in some phases of the pulsation cycle but become sharper than it in the remaining phases for the all runs. When $\sqrt{\omega'}$ increases over ~5.0 up to ~28.0; the sharper profiles approach to the Blasius's distribution but the blunter profiles drop below or underestimate it at the central core region (i.e., $r/R<0.4$) and move up to the wall in the outer region (i.e., $0.6<r/R<1.0$). The experimental velocity profiles for the phases in the second half of the accelerating period and for the phases in the first half of the decelerating period approach quite close of the wall in the outer region and show almost a peak of rectangular-like velocity profile at $r/R\approx0.85$ when $\sqrt{\omega'}\approx28.0$. This fact of the experimental and the computational velocity profiles in the present study show that; the limiting value of the dimensionless frequency parameter between the intermediate and the inertia dominant regions of the laminar-pulsatile pipe flow can be accepted as $\sqrt{\omega'}\approx28.0$ and the peak of the velocity profile tends to gradually approach the pipe wall when $\sqrt{\omega'}$ increases from ~5.0 to the upper limit, ~28.0 of the intermediate region. These facts are firstly clarified by means of both the systematic velocity measurements and the finite-volume based computations in this study.

ACKNOWLEDGEMENTS

This study was financially supported by the Research Fund of the University of Gaziantep in terms of research projects coded as MF.97.04 and MF.07.06.

REFERENCES

ANSYS Inc., Boundary Conditions, *in Introductory Fluent Notes*, 4-8, 2006.

Atabek, H. B., and Chang, C. C., Oscillatory flow near the entry of a circular tube, *Zeitschrift für angewandte Mathematik und Physik* 12, 185-201, 1961.

Atabek, H. B., Chang, C. C., and Fingerson, L. M., Measurement of laminar oscillatory flow in the inlet of a circular tube, *Physics of Medicine Biology* 9, 219-227, 1965.

Balmer, R. T., and Fiorina, M. A., Unsteady flow of an inelastic power-law fluid in a circular tube, *Journal of Non-Newtonian Fluid Mechanics* 7, 189-198, 1980.

Brown, F. T., The transient response of fluid lines, Journal of Basic Engineering, *Transactions of the ASME, Series D* 84, 547-553, 1962.

Carpinlioglu, M. O., and Gundogdu, M. Y., A critical review on pulsatile pipe flow studies directing towards future research topics, *Flow Meas Instrum* 12, 163-174, 2001a.

Carpinlioglu, M. O., and Gundogdu, M. Y., Presentation of a test system in terms of generated pulsatile flow characteristics, *Flow Meas Instrum* 12, 181-190, 2001b.

Denison, E. B., Pulsating laminar flow measurements with a directionally-sensitive laser velocimeter, Ph.D. Dissertation, *Purdue University*, 1970.

Denison, E. B., Stevenson, W. H., and Fox, R. W., Pulsating laminar flow measurements with a directionally sensitive laser velocimeter, *AIChE Journal* 17, 781-787, 1971.

Donovan, F. M., Taylor, B. C., and Su, M. C., One-dimensional computer analysis of oscillatory flow in rigid tubes, *Journal of Biomechanical Engineering* 113, 476-484, 1991.

Donovan, F. M., McIlwain, R. W., Mittmann, D. H., and Taylor, B.C., Experimental correlations to predict fluid resistance for simple pulsatile laminar flow of

incompressible fluids in rigid tubes, *Journal of Fluids Engineering* 116, 516-521, 1994.

D'Souza, A. F., and Oldenburger, R., Dynamic response of fluid lines, *Journal of Basic Engineering, Transactions of the ASME, Series D* 86, 589-598, 1964.

Farell, C., and Youssef, S., Experiments on turbulence management using screen and honeycombs, *Trans. A.S.M.E, J. Fluids Engng* 118, 26-32, 1996.

Florio, P. J., and Mueller, W. K., Development of a periodic flow in a rigid tube, *Journal of Basic Engineering, Transactions of the ASME, Series D* 90, 395-399, 1968.

Gerlach, C. R., and Parker, J. D., Wave propagation in viscous fluid lines including higher model effect, *Journal of Basic Engineering, Transactions of the ASME, Series D* 89, 782-788, 1967.

Gerrard, J. H., and Hughes, M. D., The flow due to an oscillating piston in a cylindrical tube: A comparison between experiment and a simple entrance flow theory, *J Fluid Mech* 50, 97-106, 1971.

Gundogdu, M. Y., and Carpinlioglu, M. O., Present state of art on pulsatile flow theory. Part 1: laminar and transitional flow regimes, *JSME International Journal* 42, 384-397, 1999.

Gundogdu, M. Y., An experimental investigation on pulsatile pipe flows, Ph.D Thesis, *University of Gaziantep*, Department of Mechanical Engineering, 2000.

Gundogdu, M. Y., and Carpinlioglu, M. O., An interactive data acquisition and control system coupled on a pulsatile pipe flow test rig, *Measurement and Control* 35, 43-46, 2002.

Harris, J., Peer, G., and Wilkinson, W. L., Velocity profiles in laminar oscillating flow in tubes, *J. Phys. E. J. Sci. Instrum.* 2, 913-916, 1969.

Hershey, D., and Song, G., Friction factors and pressure drop for sinusoidal laminar flow of water and blood in rigid tubes, *AIChE Journal* 13, 491-496, 1967.

Hino, M., Sawamato, M., and Takasu, S., Experiments on transition to turbulence in an oscillatory pipe flow, *J Fluid Mech* 75, Part 2, 193-207, 1976.

Jayasinghe, D. A. P., Letelier, S. M., and Leutheusser, H.J., Frequency-dependent friction in oscillatory laminar pipe flow, *Internaional Journal of Mechanical Sciences* 16, 819-827, 1974.

Jung, J., Lyczkowski, R. W., Panchal, C. B., and Hassanein, A., Multiphase hemodynamic simulation with pulsatile flow in a coronary artery, *J. Biomech.* 39, 2064-2073, 2006.

Linford, R. G., and Ryan, N. W., Pulsatile flow in rigid tubes, *Journal of Applied Physiology* 20, 1078-1082, 1965.

Linke, W., and Hufschmidt, W., Wärmeübergang bei pulsierender Strömung (Heat transfer in pulsating flow), *Chem. Ing. Techn.* 30 159-165, 1958.

Loehrke, R. L., and Nagib, H. M., Control of free stream turbulence by means of honeycombs: A balance between suppression and generation, *Trans. A.S.M.E, J. Fluids Engng* 98, 342-353, 1976.

Muto, T., and Nakane, K., Unsteady flow in circular tube; Velocity distribution of pulsatile flow, *Bulletin of JSME* 23, 1990-1996, 1980.

Ohmi, M., Usui, T., Fukawa, M., and Hirasaki, S., Pressure and velocity distributions in pulsating laminar pipe flow, *Bull Jpn Soc Mech Eng* 19, 298-306, 1976.

Ohmi, M., Iguchi, M., and Usui, T., Flow pattern and frictional losses in pulsating pipe flow. Part 5: Wall shear stress and flow pattern in a laminar flow, *Bull Jpn Soc Mech Eng* 24, 75-81, 1981a.

Ohmi, M., and Iguchi, M., Flow pattern and frictional losses in pulsating pipe flow. Part 6: Frictional losses in a laminar flow, *Bulletin of the JSME* 24, 1756-1763, 1981b.

Ohmi, M., Iguchi, M., and Urahata, I., Transition to turbulence in a pulsatile pipe flow. Part 1; Wave forms and distribution of pulsatile velocities near transition region, *Bull Jpn Soc Mech Eng* 25, 182-189, 1982.

Richardson, E. G., The amplitude of sound waves in resonators, *Proceedings of the Physical Society* 40, 206-220, 1928.

Richardson, E. G., and Tyler, E., The transverse velocity gradient near the mouths of pipes in which an alternating or continuous flow is established, *Proceedings of the Physical Society* 42, 1-15, 1930.

Rosenhead, L., *Laminar Boundary Layers*, Oxford University Press, 1963.

Sexl, T., Uber den von E. G. Richardson entdeckten 'Annulareffekt', *Zeitschrift für Physik* 61, 349-362, 1930.

Steinman, D. A., Image-based computational fluid dynamics modeling in realistic arterial geometries, *Ann. Biomed. Eng.* 30, 483-497, 2002.

Szymanski, P., Some exact solutions of the hydrodynamic equation of a viscous fluid in the case of a cylindrical tube, *J. Math. Pure Appl.* 11, 67-107, 1932.

Uchida, S., The pulsating viscous flow superposed on the steady laminar motion of incompressible fluids in a circular pipe, *Z. Angew. Math. Phys.* 7, 403-422, 1956.

Unsal, B., Ray, S., Durst, F., and Ertunc, O., Pulsating laminar pipe flows with sinusoidal mass flux variations, *Fluid Dynamics Research* 37, 317-333, 2005.

Womersley, J. R., Method for the calculation of velocity, rate of flow and viscous drag in arteries when the pressure gradient is known, *Journal of Physiology* 127, 553-563, 1955.

Womersley, J. R., An elastic tube theory of pulse transmission and oscillatory flow in mammalian arteries, *WADC Technical Report TR56-614*, 1957.

Yilmaz, F., and Gundogdu, M. Y., A critical review on blood flow in large arteries; relevance to blood rheology, viscosity models, and physiologic conditions, *Korea Aust Rheol J* 20, 197-211, 2008.

Yilmaz, F., and Gundogdu, M. Y., Analysis of conventional drag and lift models for multiphase CFD modeling of blood flow, *Korea Aust Rheol J* 21, 161-173, 2009.

Zhao, T., Sanada, K., Kitagawa, A., and Takenaka, T., Real time measurement for high frequency pulsating flow rate in a pipe, *J Dyn Syst Meas Contr* 112, 762-768, 1990.

Zielke, W., Frequency-dependent friction in transient pipe flow, *Journal of Basic Engineering, Transactions of the ASME, Series D* 90, 109-115, 1968.